ACS OMEGA

Open Access

This article is licensed under CC-BY-NC-ND 4.0

http://pubs.acs.org/journal/acsodf

Article

Application of Odd-Order Derivatives in Fourier Transform Nuclear Magnetic Resonance Spectroscopy toward Quantitative Deconvolution

Shu-Ping Chen,*,‖ Sandra M. Taylor,‖ Sai Huang, and Baoling Zheng

Cite This: *ACS Omega* 2024, 9, 36518−36530

Read Online

ACCESS | Metrics & More | Article Recommendations | Supporting Information

ABSTRACT: When Fourier transform (FT) spectrum peaks are overlapped, primary maxima of odd-order derivatives can be used to evaluate their independent intensities. We studied the feasibility of higher odd-order derivatives on Lorentzian peak shape and magnitude peak shape. Simulation studies for FT nuclear magnetic resonance (NMR) spectroscopy demonstrated good results toward quantitative deconvolution of overlapping FT spectrum peaks. Although it is not so desirable to deconvolute special line shapes such as Gaussian, Voigt, and Tsallis profiles, the odd-order derivatives exhibit a bright future compared to even-order derivatives. An application example of practical NMR spectroscopy with ethylbenzene isomers is presented. White Gaussian noises were added to the simulated spectra at two different signal-to-noise ratios (20 and 40). Kauppinen's denoising and smoothing algorithms can effectively remove interference of the noise and help to have good deconvoluting results using the odd-order derivatives. We compared features of our approach with popular deconvolution sharpening algorithms and conducted a comparison study with Kauppinen's Fourier self-deconvolution. Our approach has a better dynamic range of peak intensities and is not sensitive to the sampling rates. Other common deconvolution methods are also discussed briefly.

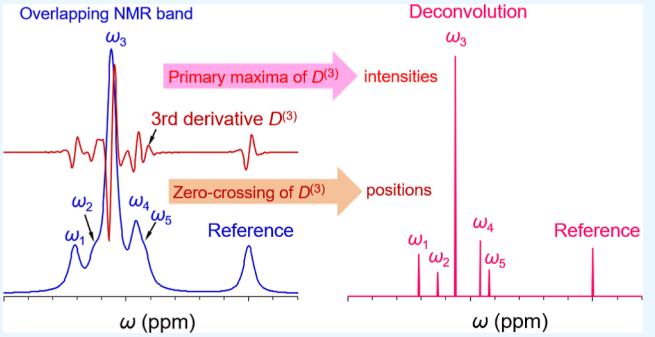

1. INTRODUCTION

Deconvolution of overlapping peaks is a method to overcome the upper bounds of spectroscopic performance. An advantage of Fourier transform (FT) in spectroscopy is that the periodic time signals can be converted to symmetric bell-shape peaks. In this paper, we developed a novel deconvolution approach using odd-order derivatives for overlapping spectral bands, in perspective of FT nuclear magnetic resonance (NMR) (FT-NMR) spectroscopy. The general principle described here may also be applicable to other FT spectroscopies.

The aim of superimposing the FT is to improve spectral resolution by folding a FT peak about its symmetric axis or center to double its peak intensity and reduce its width by half (see illustration in Section S1 of Supporting Information).[1,2] It is difficult to convolute the superimposition functions on FT in the time domain t from thousands to millions of data points without prior knowledge about the signal waves. Alternatively, this can be accomplished in the frequency domain ω by derivative spectroscopy using stepwise superimposition.[2] We conducted a stair-like configuration to link identified peak vertices and raise every step at each peak vertex by 2. This configuration is termed the stepwise superimposition function $S_k(\omega)$

$$S_k(\omega) = 2(k + a) \qquad k, a \in +Z \tag{1}$$

where $k = 0, 1, ..., N$ for N peaks in an overlapping band and a is a positive integer ≥ 0 $(+Z)$ because initial step $S_0(\omega)$ may not be a zero baseline. Its principle is exemplified in Figure 1 regarding the 4 overlapping peaks of a conventional FT spectrum $F(\omega)$: ω_1, ω_2, ω_3, and ω_4. The brownish steps shown on the top of Figure 1 are stepwise superimpositions, progressively from the left side fold to the right (that is, right-superimpose $\omega_1 \rightarrow \omega_4$). Of course, we can also perform a left superimposition $\omega_4 \rightarrow \omega_1$ in reverse order. The "stepwise" here means that the step intervals (i.e., peak separations) are varied.

Multiplication of the spectrum $F(\omega)$ with its stepwise superimposition function $S_k(\omega)$ links each step to its corresponding peak vertex. There are $k = N+1$ steps for N overlapping peaks. After taking first-order differentials (or derivatives) of the multiplication $\{F(\omega)\cdot S_k(\omega)\}$ as per the product rule

Received: May 13, 2024
Revised: July 28, 2024
Accepted: July 31, 2024
Published: August 14, 2024

© 2024 The Authors. Published by American Chemical Society

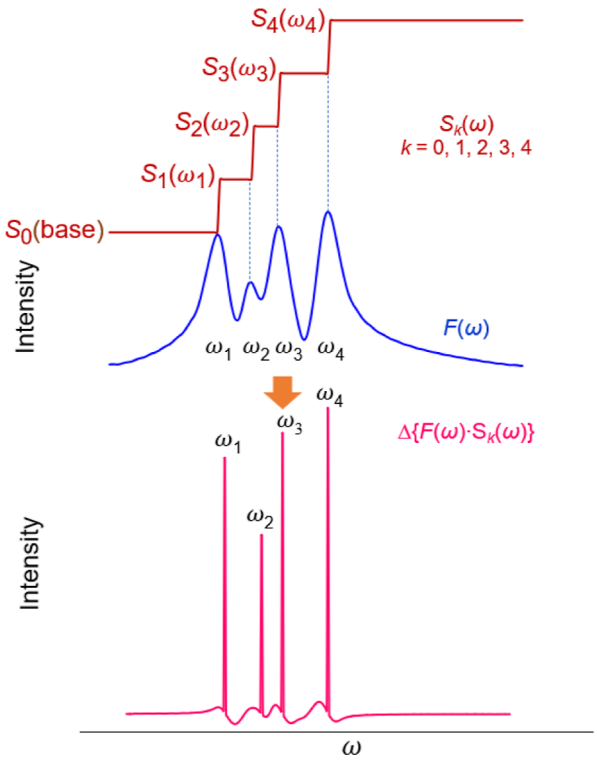

Figure 1. Middle blue spectrum is a simulated conventional FT spectrum $F(\omega)$, composed of 4 overlapping peaks ω_1, ω_2, ω_3, and ω_4. Top brownish configuration is a stepwise superimposed function $S_k(\omega)$ (k = 0, 1, 2, 3, 4) from right toward left ($\omega_1 \rightarrow \omega_4$). Starting at the lowest step S_0 (base of peak ω_1), the first step S_1 at the peak vertex of ω_1 by a factor 2, and so on progressively to the following peak vertices step by step. Differential of the multiplications, $\Delta\{F(\omega)\cdot S_k(\omega)\}$, gives a stepwise right-superimposed differential spectrum (pink spectrum bottom).

$$\Delta\{F(\omega)\cdot S_k(\omega)\} = \Delta S_k(\omega)\cdot F(\omega) + S_k(\omega)\cdot\Delta F(\omega) = 2F(\omega_j) + S_k(\omega)\Delta F(\omega) \quad (2)$$

because $\Delta S_k(\omega) = 2$ at peak vertex ω_j, where j = 1, 2, ..., N for N peaks in a spectrum. Since $\Delta S_k(\omega) = 0$ is other than the peak vertex, we removed $S_k(\omega)$ from the last term of eq 2 to obtain a first-order differential background $\Delta F(\omega)$. Thus, we obtain two types of spectral data

$$\left.\begin{array}{l}\text{peak vertices } 2F(\omega)_j \\ \text{background } \Delta[F(\omega)]\end{array}\right\} \quad (3)$$

The four overlapped peaks are sharply resolved by stepwise superimposition of the pink spectra at the bottom of Figure 1 through right-superimposition (or left-superimposition) to double their peak intensities with respect to first-order differential background (this refers to an excel schema in Section S2 of the Supporting Information).

Implementation of the stepwise superimposed derivative relies on well-known features of FT spectroscopy:[3] symmetric profiles with identical full width at half-maximum (FWHM) and peak height proportional to signal amplitude. The major drawback of this strategy is to superimpose each overlapping peak on their apparent heights, not their true ones. This is a consequence of the implementation of the superimposition operation in the frequency domain rather than in the time domain. Derivatives are often used to deconvolute the overlapping peaks qualitatively and quantitatively.[4] The even-order derivatives, especially second-order and fourth-order derivatives, are universally preferred in the spectroscopic community because of their centric maximums around their parent peaks if the spectral derivatives are well-convergent.[4,5] In fact, odd-order derivatives of a symmetric peak have more unique features: their centers pass across zero and display antisymmetric maxima. Nevertheless, their derivative maxima are proportional to their parent peak heights, as are those of even-order derivatives. We probed odd-order (higher than third-order) derivatives toward quantitative deconvolution of the overlapping FT bands based on these peculiarities.

The derivative algorithm faithfully obtains variables of the original spectrum point by point to predict the behaviors after the overlapping, which is similar to the curve fitting strategy employed in spectral deconvolutions among a multitude of current deconvolution methods. The deconvolution features of the odd-order derivatives will be studied and compared later with some of the popular deconvolution methods. A remarkable advantage of derivative spectroscopy is that constant and lower-order noises are eliminated or reduced by higher-order derivatives.[4]

2. HIGH-ORDER DIFFERENTIAL DECONVOLUTION

A general formula of the nth-order derivative $D^{(n)}$ discrete spectroscopy in a sampling interval of $\Delta\omega$ as Leibniz rule is[4,6]

$$D^{(n)}_{\omega+\delta(\Delta\omega/2)} = \frac{1}{(\Delta\omega)^n}\sum_{m=0}^{n} C_n^m(-1)^m A_{\omega+[(n+\delta-2m)/2]\Delta\omega} \quad (4)$$

where $C_n^m = n(n-1)...(n-m+1)/m!$, binominal coefficients; δ = 0 for even n, and δ = 1 for odd n; a general factor; and $A_{\omega+[(n+\delta-2m)/2]\Delta\omega}$, intensity at frequency $\omega + [(n + \delta-2m)/2]\Delta\omega$. For the third-order derivative, n = 3 and m = 0, 1, 2, 3

$$D^{(3)}_{\omega+\Delta\omega/2} = (A_{\omega+2\Delta\omega} - 3A_{\omega+\Delta\omega} + 3A_{\omega} - A_{\omega-\Delta\omega})/(\Delta\omega)^3$$

The full binominal coefficients of third-order derivatives to tenth-order derivatives are available in Section S3 of the Supporting Information for readers' convenience.

Recently, Belkić and Belkić [2018, 2019] employed very high-order derivatives (up to 50th order) in the fast Padé transform of magnetic resonance spectroscopy to quantify cancer biomarkers.[7] Their Padé transforms utilized prior knowledge about signal frequencies to reconstruct the spectra by multiple iterative averaging to match the acquired time signal polynomial.[8,9] Belkićs revealed that quantitative deconvolution can be achieved by higher-order derivatives as more neighboring data are analyzed, together with each peak vertex.

2.1. Odd-Order Derivatives of Overlapped Lorentzian Peaks. FT spectroscopy (or spectrometry) refers to a spectroscopic method with Fellgett's multiplex advantage: gain factor of signal-to-noise ≫1 related to its scanning type.[10] Theoretically, its spectrum peak shape is a Lorentzian profile[10]

$$L(\omega) = \frac{A_j\sigma}{\sigma^2 + (\omega - \omega_j)^2} \quad (5)$$

where ω_j is signal frequency; A_j is its peak intensity; and σ is the attenuation factor for a harmonic signal $f(t) = 2A_j e^{-\sigma t}\cos\omega_j t$. Theoretical FWHM of a FT peak = 2σ.[10] We calculated the major characteristics of its derivatives up to fifth-order in Table

https://doi.org/10.1021/acsomega.4c04536
ACS Omega 2024, 9, 36518−36530

1, where $D^{(n)}$ denotes the nth derivative of the Lorentzian profile. The maximum heights of even- and odd-order derivatives are both proportional to independent peak intensity A_j. Odd-order derivatives exhibit two antisymmetric primary maxima (PM) that respond to the overlapping differently. Nevertheless, their FWHM is much narrower than that of the PM of their subsequent even-order derivatives.

Table 1. Primary Maximum (1st Max) and Secondary Maximum (2nd Max) of Derivatives up to 5th-Order for a Lorentzian Peak $L(\omega)$

	1st max		2nd max	
$D^{(n)}$	$\omega - \omega_j$	height	$\omega - \omega_j$	height
$D^{(1)}$	$\pm 0.577\sigma$	$\mp 0.650A_j/\sigma^2$	——	——
$D^{(2)}$	0	$-2A_j/\sigma^3$	$\pm\sigma$	$+0.5A_j/\sigma^3$
$D^{(3)}$	$\pm 0.325\sigma$	$\pm 4.669A_j/\sigma^4$	$\pm 1.376\sigma$	$\mp 0.421A_j/\sigma^4$
$D^{(4)}$	0	$+24A_j/\sigma^5$	$\pm 0.577\sigma$	$-10.125A_j/\sigma^5$
$D^{(5)}$	$\pm 0.228\sigma$	$\mp 100.459A_j/\sigma^6$	$\pm 0.797\sigma$	$\pm 21.428A_j/\sigma^6$

It is noteworthy that $D^{(3)}$ of the Lorentzian peak has the smallest height ratio of second max to first max (only 9.0% calculated from Table 1). The height ratios of the other derivative orders are over 20%. The same observations were portrayed in the beginning part of Dubrovkin's "Derivative Spectroscopy".[4] Third-order derivatives can thus achieve more accurate deconvolution and should be used to study overlapping bands by FT spectroscopy. FT spectroscopic peaks are actually close to the Lorentzian profile.[10] The apodization broadened peak widths and decreased peak heights to a certain extent. Many physical and chemical factors can affect the peak widths and shapes.[4] We utilized simulation to estimate the deconvolution of the overlapping bands with odd-order derivatives due to a limitless overlapping manifold. We defined the separation between the two peaks ω_j and ω_{j+1} ($\omega_{j+1} > \omega_j$) in a half of FWHM σ as

$$\omega_{j+1} - \omega_j = \gamma\sigma \tag{6}$$

where γ is the spectral overlapping degree rigorously stipulated by Vandeginste and De Galan.[11]

We simulated ^{13}C NMR spectroscopy[12] as the blue spectrum shown in Figure 2, where there are absorption peaks: ω_1, ω_2, ω_3, ω_4, and ω_5 overlapped into a band, and a well separated peak ω_6 as a reference for the sake of the evaluation (refers to Section S4 of Supporting Information for their simulated free induction decay (FID) signal). The overlapped peaks are evaluated against the reference peak ω_6 by their third-order derivatives (the brown curve in Figure 2) since the third-order derivatives have minimum satellites' influence and their dispersive PMs underwent different overlapping effects.

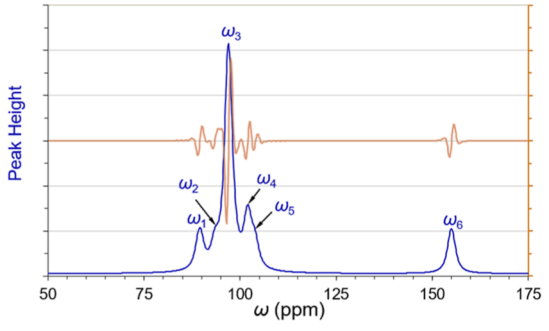

Figure 2. Simulated FT spectrum composed of six absorption peaks (depicted in blue): ω_1, ω_2, ω_3, ω_4, and ω_5 are merged into a band; and ω_6 is separated well from the others as a reference for intensity evaluation. Brown curve is their 3rd-order derivative $D^{(3)}$ spectrum.

The reference peak intensity is always normalized in this study to make the calculation simpler. The master simulation parameters are semi-FWHM σ = 1.23 after being apodized by a 3-term Blackman−Harris window; there are two different sampling rates for comparison: 4 times and 16 times of Nyquist frequency (f_N). The simulated peak characteristics and their deconvolution results are listed in Table 2. The five overlapping peaks are deconvoluted very well in the simulation study. The deviations of their independent intensities generally are not more than ±5% for overlapping degrees 2.8 to 4.1. The accuracy declines when the overlapping degree of a peak ≤2.0 and intensity ratio of its adjacent peak ≥2. A higher sampling rate helps to display peak amplitude and reduces dilation. The evaluation accuracy is obviously not improved as the sampling rate was raised from 4 to 16 times Nyquist frequency. The evaluation using the third-order derivative is fortunately not susceptible to sampling rate. The PM with less overlapping effect always gives a good evaluation of A_j. When front A_j and back A_j are similar, it is better to average them for reliability. The well separated peak ω_6 acts as an internal reference standard and is normalized in Table 2. Its independent peak intensity will be solved later (referring to Section S5 of the Supporting Information for the related Excel calculations).

2.2. Odd-Order Derivatives of Overlapped Gaussian and Related Peaks. The Gaussian peaks can be deliberately generated by FT spectroscopy. Full width at baseline of a Gaussian profile is about 6σ (note: σ = semi-FWHM) in contrast to the long tailing of a Lorentzian profile. Thus, the overlapping of Gaussian peaks is much weaker than that of Lorentzian peaks under the same circumstances because the slope of a Gaussian profile varies more sharply. For a typical Gaussian peak $G(\omega)$ at ω_j with intensity A_j

$$G(\omega) = A_j e^{-\ln 2[(\omega-\omega_j)/\sigma]2}/\sigma \tag{7}$$

we calculated the nth-derivative up to $D^{(5)}$ in Table 3 for its PM (1st max) and secondary maxima (2nd max).

Consequently, derivatives of $G(\omega)$ demonstrate much stronger satellite maxima than those of Lorentzian $L(\omega)$. Their height ratios of second max to first max are all over 27%. Therefore, the PM of $G(\omega)$ is not suitable to evaluate closely overlapping Gaussian peaks. Overlapping doublets are elementary models in searching for related parameters in the evaluation of derivative spectroscopy (see dedicated chapter in Dubrovkin's book),[4] we simulated two overlapping Gaussian peaks, ω_1 and ω_2, at overlapping degree γ = 2.0 with a well resolved reference peak ω_3 in Figure 3. Their FWHM of 2σ = 2.0 and their independent intensity ratio of $A_1/A_2/A_3$ = 1:5:1.

The derivative satellites would cause greater interference with the PMs for the deconvolution of closely overlapping Gaussian peaks. As the above strategy for the overlapping Lorentzian peaks and FT absorption peaks, we tracked where there are fewer overlapping portions of their odd-order derivatives to implement our deconvolutions. The third-order derivative satellite maxima had been recommended to deconvolute the overlapping peaks for this reason (see p. 204 of Dubrovkin's "Derivative Spectroscopy").[4] We appreciate that the second maxima of $D^{(3)}$ achieves intensity deviations that are less than +2.1% for the overlapping Gaussian doublet with the aid of the

https://doi.org/10.1021/acsomega.4c04536
ACS Omega 2024, 9, 36518−36530

Table 2. Simulation Data of the FT Spectrum in Figure 2 and Results Evaluated by $D^{(3)}$

peak ω_j (j = 1, 2, ..., 6)		ω_1	ω_2	ω_3	ω_4	ω_5	ω_6
overlapping degree γ		3.3	2.8	4.1	1.5	41.6	——
real intensity A_j		**0.880**	**0.500**	**5.000**	**1.150**	**0.550**	1.000
$4f_N$	apparent A_j	1.118	1.121	5.172	1.624	1.044	1.094
	% deviation	+27.0%	+124.2%	+3.4%	+41.2%	+89.8%	+9.4%
	front A_j	0.893	0.492	5.030	1.100	0.544	1[a]
	% deviation	+1.5%	−1.6%	+0.6%	−4.3%	−1.1%	
	back A_j	0.875	0.767	4.999	1.078	0.394	1[a]
	% deviation	−0.6%	+53.4%	−0.0%	−6.3%	−28.4%	
$16f_N$	apparent A_j	1.050	1.052	5.138	1.560	1.016	1.026
	% deviation	+19.3%	+110.4%	+2.8%	+35.7%	+84.7%	+2.6%
	front A_j	0.899	0.489	5.003	1.094	0.589	1[a]
	% deviation	+2.2%	−2.2%	+0.1%	−4.9%	+7.1%	
	back A_j	0.883	0.729	4.995	1.159	0.407	1[a]
	% deviation	+0.3%	+45.8%	−0.1%	+0.8%	−26.0%	

[a]Peak ω_6 is normalized to one in the intensity evaluation.

Table 3. Primary Maximum (1st Max) and Secondary Maximum (2nd Max) of Derivatives up to 5th-Order for a Gaussian Peak $G(\omega)$ Described by eq 7

	1st max		2nd max	
$D^{(n)}$	$\omega - \omega_j$	height	$\omega - \omega_j$	height
$D^{(1)}$	$\pm 0.849\sigma$	$\mp 0.714A_j/\sigma 2$	——	——
$D^{(2)}$	0	$-1.386A_j/\sigma 3$	$\pm 1.471\sigma$	$+0.619A_j/\sigma 3$
$D^{(3)}$	$\pm 0.630\sigma$	$\pm 2.253A_j/\sigma 4$	$\pm 1.983\sigma$	$\mp 0.612A_j/\sigma 4$
$D^{(4)}$	0	$+5.765A_j/\sigma 5$	$\pm 1.151\sigma$	$-3.565A_j/\sigma 5$
$D^{(5)}$	$\pm 0.524\sigma$	$\mp 13.086A_j/\sigma 6$	$\pm 1.605\sigma$	$\pm 5.707A_j/\sigma 6$

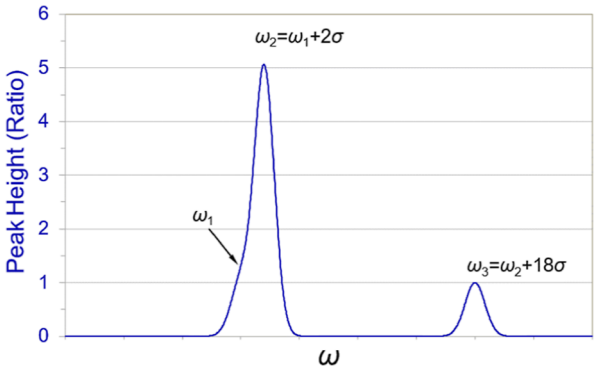

Figure 3. Simulated doublet composed of two Gaussian peaks, ω_1 and ω_2, at an overlapping degree γ = 2.0. Well separated Gaussian peak, ω_3 (γ = 18.0), is used as an internal reference.

reference peak ω_3, as shown in Table 4. However, the second maxima of $D^{(5)}$ provide poorer deconvolution because the gap between their second maxima ($\pm 1.605\sigma$, see Table 3) is narrower than that of $D^{(3)}$ ($\pm 1.983\sigma$, see Table 3). When overlapping of the spectrum peaks become closer (γ < 2.0), fractional derivatives[4] and curve fitting[13] have advantages in the evaluation of the overlapping Gaussian peaks. The Voigt shape is a convolution of the Gaussian and Lorentzian functions.[4] We found that dispersive PMs of $D^{(5)}$ are valid for deconvolution of Voigt doublets when they have more than one-third of the Lorentzian component. A similar option to Tsallis shapes,[4] the partition between Gaussian and Lorentzian will govern the evaluation feasibility for overlapping Tsallis peaks using the odd-order derivatives, either PM or second max.

Table 4. Evaluation of Overlapping Gaussian Doublet by Odd-Order Derivatives

Gaussian peak	ω_1	ω_2	ω_3
γ	2.0	18.0	–
real A_j (j = 1, 2, 3)	1	5	1
apparent A_j	1.313	5.065	1.000
(% deviation)	(+31.3%)	(+1.3%)	(0.0%)
2nd max of $D^{(3)}$	1.021	5.004	1[a]
(% deviation)	(+2.1%)	(+0.0%)	
2nd max of $D^{(5)}$	0.849	4.966	1[a]
(% deviation)	(−15.1%)	(−0.7%)	

[a]Intensity of ω_3 is normalized as 1 in the evaluation to compare front maxima for ω_1 and back maxima for ω_2.

2.3. Odd-Order Derivatives of Overlapped Magnitude Peaks.

Magnitude mode is favored when controlling the phase shifts in FT spectroscopy. The magnitude shape $M(\omega)$ of a single peak ω_j with intensity A_j as the acquisition time T is long[10]

$$M(\omega) = \left| \frac{A_j\sigma}{\sigma^2 + (\omega - \omega_j)^2} - i\frac{A_j(\omega - \omega_j)}{\sigma^2 + (\omega - \omega_j)^2} \right| = \frac{A_j}{\sqrt{\sigma^2 + (\omega - \omega_j)^2}} \quad (8)$$

The magnitude mode is the absolute value of its independent Lorentzian peak with an imaginary dispersive peak. When two magnitude peaks ω_1 and ω_2 with intensities A_1 and A_2 are overlapped and if their phase shifts are relatively small, their intensity sums are[14]

$$\left| \frac{A_1\sigma}{\sigma^2 + (\omega - \omega_1)^2} + \frac{A_2\sigma}{\sigma^2 + (\omega - \omega_2)^2} - i\left[\frac{A_1(\omega - \omega_1)}{\sigma^2 + (\omega - \omega_1)^2} + \frac{A_1(\omega - \omega_2)}{\sigma^2 + (\omega - \omega_2)^2} \right] \right| = \left[\frac{A_1^2}{\sigma^2 + (\omega - \omega_1)^2} + \frac{A_1^2}{\sigma^2 + (\omega - \omega_2)^2} + \frac{2A_1A_2[\sigma^2 + (\omega - \omega_1)(\omega - \omega_2)]}{[\sigma^2 + (\omega - \omega_1)^2][\sigma^2 + (\omega - \omega_2)^2]} \right]^{\frac{1}{2}} \quad (9)$$

https://doi.org/10.1021/acsomega.4c04536
ACS Omega 2024, 9, 36518−36530

Peak width of the magnitude mode is broadened by $\sqrt{3}$ corresponding to its Lorentzian component and displays more tailing than the Lorentzian profile. Another drawback of the magnitude mode is that overlapped magnitude peaks are nonadditive.[14] Therefore, independent intensities of the overlapping magnitude peaks cannot be assessed by comparing derivative maxima (either odd- or even-order), as in the above approach for Lorentzian and Gaussian peaks. When examining odd-order derivatives $D^{(n)}$ up to ninth-order in Table 5, $D^{(3)}$ of a magnitude peak ω_j also shows minimum ratio (~6.3%) of 2nd max relative to its PM (1st max).

Table 5. Primary Maximum (1st Max) and Secondary Maximum (2nd Max) of Odd-Order Derivatives for a Magnitude Peak $M(\omega)$

	1st max		2nd max	
$D^{(n)}$	$\omega - \omega_j$	height	$\omega - \omega_j$	height
$D^{(1)}$	$\pm 0.707\sigma$	$\mp 0.385A_j/\sigma^2$	——	——
$D^{(3)}$	$\pm 0.362\sigma$	$\pm 1.932A_j/\sigma^4$	$\pm 1.694\sigma$	$\mp 0.122A_j/\sigma^4$
$D^{(5)}$	$\pm 0.246\sigma$	$\mp 33.678A_j/\sigma^6$	$\pm 0.881\sigma$	$\pm 6.298A_j/\sigma^6$
$D^{(7)}$	$\pm 0.187\sigma$	$\pm 1268.236A_j/\sigma^8$	$\pm 0.618\sigma$	$\mp 371.466A_j/\sigma^8$
$D^{(9)}$[a]	$\pm 0.150\sigma$	$\mp 83452A_j/\sigma^{10}$	$\pm 0.481\sigma$	$\pm 31495A_j/\sigma^6$

[a]The values of the 9th derivative were estimated by numerical calculations.

It is worth noting that the gaps between the two PM ($\omega - \omega_j$) narrow progressively with increasing derivative orders, and the height absolute ratios of the PM (positive versus negative) are always to be 1. When the peaks overlap, their peak intensities are dilated and accordingly the PM of their derivatives will be deformed with the overlapping. We define the primary maximum ratio (PMR) of the peak derivatives as

$$\text{PMR} = |\text{smaller PM/larger PM}| \tag{10}$$

where the smaller and larger maxima are specified as their absolute amplitudes, regardless of being positive or negative. Because of overlapping dilation, the apparent peak intensity $A_{j(\text{apparent})}$ of a peak ω_j is larger than its independent intensity A_j. We speculated an approximation relation for overlapping magnitude peaks according to their broad tailing feature

$$A_j/A_{j_{(\text{apparent})}} \approx \text{PMR} \tag{11}$$

To affirm eq 11, we studied two overlapping FT magnitude peaks ω_1 and ω_2 with 4 times of the Nyquist frequency and apodized the spectrum by a 3-term Blackman-Harris window. The doublet peaks are separated at first at an overlapping degree $\gamma = 8.0$. Intensity A_1 of peak ω_1 was fixed and normalized as one. We gradually varied the intensity ratio A_2/A_1 from 0 to 30. As displayed in Figure 4, the calculated $D^{(3)}$ PMR of peak ω_1 is pertinent until intensity ratio A_2/A_1 is about 11, but its $D^{(5)}$ PMR is irrelevant.

When two magnitude peaks are overlapped more closely at $\gamma = 2.3$ as displayed in Figure 5, PMRs of $D^{(5)}$ are valid for intensity ratios up to $A_2/A_1 \approx 2$. It will be appropriate by averaging PMRs of $D^{(3)}$ and $D^{(5)}$ within a range of $A_2/A_1 \approx 2$ to 4.4 (deviation <2.0%). From the above simulation analysis of overlapping magnitude doublets, we realized that the real intensity of an overlapped magnitude peak could be evaluated with a PMR of $D^{(3)}$ or $D^{(5)}$ or both $D^{(3)}$ and $D^{(5)}$, depending on how close its neighbor(s) are. We extrapolated this supposition about eq 11 to

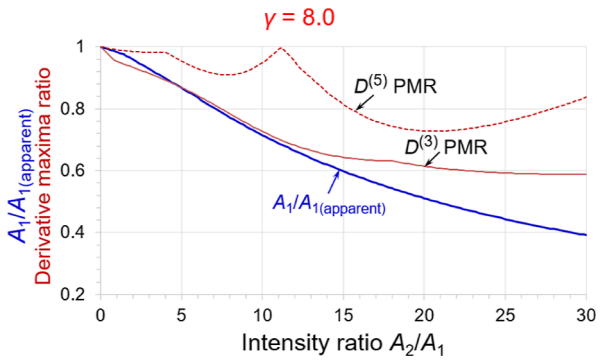

Figure 4. Intensity variation $A_1/A_{1(\text{apparent})}$ of peak ω_1 in a magnitude doublet at overlapping degree $\gamma = 8.0$ with its PMRs of $D^{(3)}$ and $D^{(5)}$ as a function of overlapping intensity ratios A_2/A_1.

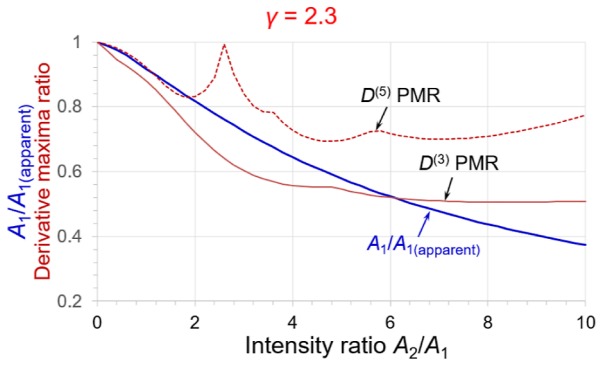

Figure 5. Intensity variation $A_1/A_{1(\text{apparent})}$ of peak ω_1 in a magnitude doublet at an overlapping degree $\gamma = 2.3$ with its PMRs of $D^{(3)}$ and $D^{(5)}$ as a function of overlapping intensity ratio A_2/A_1.

multiple overlapping peaks and verified it by the following numerical simulation.

We proceeded with the overlapping scenario of Figure 2 and converted the same six simulated peaks to magnitude modes. Since the FWHM of a magnitude peak is broadened by $\sqrt{3}$ corresponding to its absorption peak, its overlapping degree is shrunk by a factor of $\sqrt{3}$, as shown in Figure 6. The evaluation results using PMRs are listed in Table 6.

As is evident from Table 6, most evaluation results are successful (evaluation deviations ≤3.4%). The intensity of the reference peak ω_6 is precisely determined to be 1.005, which is only +0.5% deviated from its true value. On the other hand, the evaluations yield big deviations (see data for ω_2 and) when the

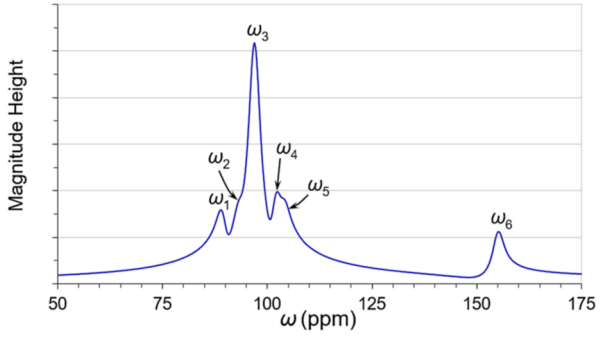

Figure 6. Simulated spectrum composed of six overlapped peaks: ω_1, ω_2, ω_3, ω_4, ω_5, and ω_6 in Figure 2 are converted to magnitude mode. They are merged more closely than in the absorption mode.

https://doi.org/10.1021/acsomega.4c04536
ACS Omega 2024, 9, 36518−36530

Table 6. Simulation Data of the Conventional FT Spectrum in Figure 6 with Sampling Rate 4 Times of Nyquist Frequency

peak ω_j (j = 1, 2, ..., 6)		ω_1	ω_2	ω_3	ω_4	ω_5	ω_6
overlapping degree γ		1.9	1.6	2.3	0.9	24.0	–
real intensity A_j		0.880	0.500	5.000	1.150	0.550	1.000
apparent A_j		1.564	1.791	5.172	1.977	1.825	1.107
% deviation		+77.7%	+258.2%	+3.4%	+71.9%	+231.8%	+10.7%
$D^{(1)}$	corrected A_j	**0.974**	**0.774**	**5.033**	**0.598**	–	**0.798**
	% deviation	+10.7%	+54.8%	+0.7%	−48.0%		−20.2%
$D^{(3)}$	corrected A_j	**0.871**	**0.819**	**5.148**	**1.371**	**1.116**	**1.005**
	% deviation	−1.0%	+63.8%	+3.0%	+19.2%	+102.9%	+0.5%
$D^{(5)}$	corrected A_j	**1.167**	**1.721**	**5.092**	**1.728**	**0.549**	**1.103**
	% deviation	+32.6%	+244.2%	+1.8%	+50.3%	−0.2%	+10.3%
$D^{(7)}$	corrected A_j	**1.177**	**1.147**	**5.126**	**1.568**	**0.598**	**1.010**
	% deviation	+33.8%	+129.4%	+2.5%	+36.3%	+8.7%	+1.0%
$D^{(9)}$	corrected A_j	**0.297**	**0.561**	**5.161**	**0.534**	**0.801**	**0.797**
	% deviation	−66.3%	+12.2%	+3.2%	−53.6%	+45.6%	−20.3%

overlapping degrees ≤1.6 and situated beside a predominant peak ω_3. Although every PMR of $D^{(1)}$ to $D^{(9)}$ is workable for the predominant peak ω_3 (the least deviation is only +0.7% given by $D^{(1)}$), $D^{(7)}$ and $D^{(9)}$ PMRs are not trustworthy for common overlapping bands to evaluate their real intensities. Higher-order derivatives bring about extensive derivative satellites and could acutely magnify Gibbs effects and spectral noises. Another merit of the PMRs is that they are also not susceptible to the sampling rate. The odd-order derivative PMRs of either Lorentzian or Gaussian profiles do not obey magnitude mode in the deconvolution. Possibly, there may be some unique cases where crowded Lorentzian or Gaussian bands do exhibit good derivative PMRs.

3. APPLICATION TO FT-NMR SPECTROSCOPY

We achieved a well-resolved 300 MHz FT NMR spectrum of ethylbenzene by implementing the stepwise differential superimposed approach.[2] The aromatic proton spin−spin coupling NMR spectrum of ethylbenzene is shown in Figure 7, where the magnitude peaks of ethylbenzene exhibited two merged bands in the spectral region of 7.0−7.4 ppm (see bottom blue spectrum of Figure 7). Eight NMR peaks corresponding to *meta*-, *ortho*-, and *para*-protons were sharply separated by the stepwise differential superimpose approach, including a big solvent peak (chloroform-*d*) against the first differential background (see top pink spectrum of Figure 7). We used odd-order derivatives to deconvolute this practical FT spectrum. A common peak width w can be determined by measuring a well resolved peak in the same spectrum or a freely induced decay factor of the NMR time signals. PMRs of odd-order derivatives ($D^{(1)}$, $D^{(3)}$, $D^{(5)}$, and $D^{(7)}$) for the nine overlapped magnitude peaks are calculated in Table 7, where their independent intensities are estimated by the PMRs of $D^{(3)}$ or .

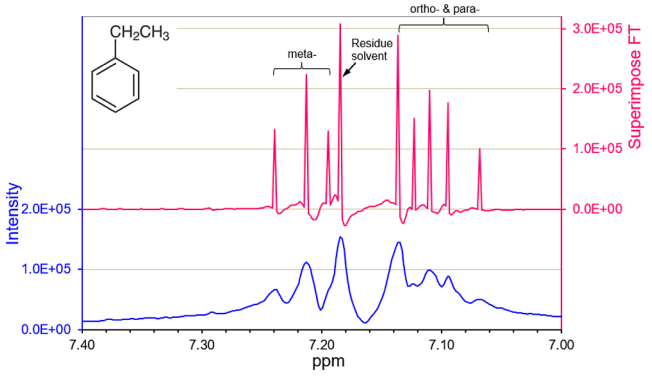

Figure 7. Blue colored spectrum is the phenyl proton spin−spin coupling 300 MHz FT NMR spectrum of ethylbenzene (chemical structure displayed in top left corner). Stepwise superimpose differential NMR spectrum of ethylbenzene (colored in pink) is overlaid on top of the figure. Nine sharp proton peaks related to the phenyl moiety and the chloroform-*d* solvent are resolved sharply.

Table 7. PMRs of the Odd-Order Derivatives from the Native FT NMR Spectrum in Figure 7

ppm	γ^a	$D^{(1)}$	$D^{(3)}$	$D^{(5)}$	$D^{(7)}$
7.068	+2.7	0.979	0.319	0.555	0.583
7.095	+1.5	0.847	0.759	0.868	0.954
7.110	+1.3	0.953	0.690	0.690	0.759
7.123	+1.3	0.577	0.278	0.319	0.327
7.136	+4.9	0.642	0.501	0.421	0.294
7.185	+1.0	0.867	0.894	0.655	0.536
7.195	+1.8	——	0.795	0.360	0.541
7.213	+2.6	0.692	0.607	0.586	0.543
7.239	——	0.616	0.368	0.465	0.301

[a]Overlapping degrees are calculated with measured FWHM 2σ = 0.02 ppm of the *meta*-proton peak at 7.213 ppm.

We chose PMR of $D^{(5)}$ to evaluate the *meta*-proton peak at 7.195 ppm because it fused into the residue solvent at 7.185 ppm. All of the other peaks were calculated on the PMRs of $D^{(3)}$. According to the PMRs of Table 7, their independent (nonoverlapping) intensities are calculated in Table 8. The PMRs are expedient evaluations to deconvolute these merged

Table 8. Independent Intensities of the Native FT NMR Spectrum in Figure 7 Evaluated by PMRs

ppm	$A_{(\text{apparent})}$	$D^{(n)}$	evaluated A
7.068	49,994	n = 3	14,636
7.095	88,530	n = 3	64,024
7.110	98,943	n = 3	65,386
7.123	75,574	n = 3	19,854
7.136	144,571	n = 3	70,390
7.185	153,942	n = 3	133,873
7.195	64,718	n = 5	21,811
7.213	111,957	n = 3	65,399
7.239	66,305	n = 3	22,855

https://doi.org/10.1021/acsomega.4c04536
ACS Omega 2024, 9, 36518−36530

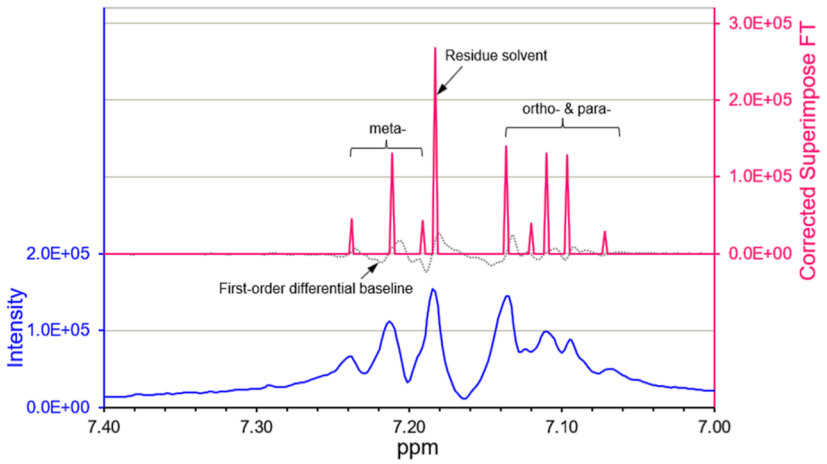

Figure 8. After the dilation evaluation, a quantitatively deconvoluted NMR spectrum is manifested on top in pink color. Bottom blue spectrum is its native 300 MHz FT NMR spectrum. First-order differential spectrum is shown in a dashed gray line, which reveals the overlapping effect.

magnitude peaks in a range of overlapping degrees 1.0 to 4.9. The deconvoluted spectrum of ethylbenzene is compatible with available literature data for 500 MHz NMR[15] and 920 MHz NMR[16] although the adjacent *ortho*- and *para*-proton peaks may exchange their spectral positions. These trivial differences may come from small interactions of adjacent ethyl protons when a magnetic field is insufficient for the NMR measurements.[15]

We can rationally smooth the spectral baseline to zero after correcting the overlapping effect (the first-order differential background in Figure 7). The intensity-corrected superimposed FT NMR spectrum (in pink color) is stacked upon its native one (blue spectrum at the bottom), as shown in Figure 8. The native NMR spectrum of ethylbenzene in Figures 7 and 8 (bottom blue one) is an appropriate model to study the overlapping issues. We observed obvious detection errors for the three peaks appearing at 7.10 to 7.15 ppm. Such errors may come from interference of the detector noises and have been rectified properly by the PMR evaluation. PMRs of the odd-order derivatives can therefore be used to evaluate the independent intensities of the overlapping peaks, and they could also become potential calibrations for detection errors.

4. NOISE INTERFERENCE AND DENOISING

Spectral noises always affect the accuracy and resolution of analytical spectroscopy. Quantitative accuracy strongly depends on the noise level in a spectrum, especially if the noises are rapidly magnified by higher-order derivatives. It is very important to expect an error threshold in a quantitative deconvolution. We can refer to the general requirements suggested by Meyer et al. for the quantitation objectives in high-performance liquid chromatography (HPLC) and capillary electrophoresis.[17] They showed that a signal-to-noise ratio (SNR) of greater than 100 was necessary for optimal precision of relative standard deviation <2%. As per the pharmacopeia criteria in method validation and technique transfer, the quantitation level should be validated to less than the error reporting threshold <2%. We at first generated a white Gaussian noise shown by a histogram in Figure 9 using Python 3.10.14 for 512 points (average = 0, standard deviation = 1, and verified by Excel). This noise was then added into the simulated spectrum of Figure 2 at SNR = 20 related to the nominal height 0.5 of the smallest peak, ω_2 (see Table 2). SNR = 200 is related to the largest peak, ω_3 (nominal height of 5.0). The additive noise

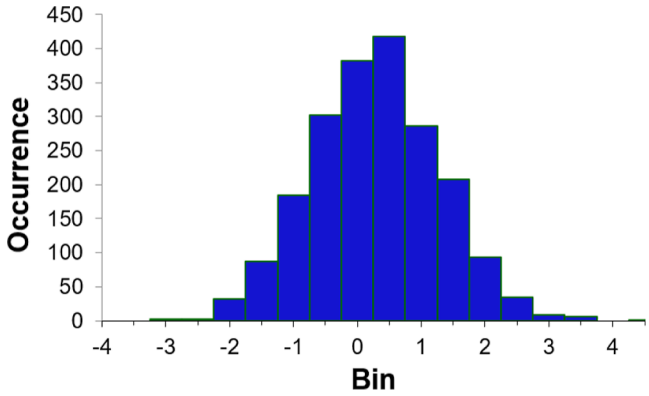

Figure 9. Histogram of the white Gaussian noise generated by Python 3.10.14 for the denoising test (redrawn by Excel).

radically corrupted the $D^{(3)}$ derivative of the synthetic spectrum, as shown in Figure 10 (refer to Section S6 of the Supporting Information for Python codes of the noise generations).

It has long been known that FT is an effective mathematical filtering for spectroscopic noises.[3] Wahab et al. designed a new denoising window—a long tailing super-Gaussian function with the FT filtering for LC.[18] Their method demonstrated great denoising achievement for the additive random noise in the chromatographic experiments. Kotani et al. just manifested that

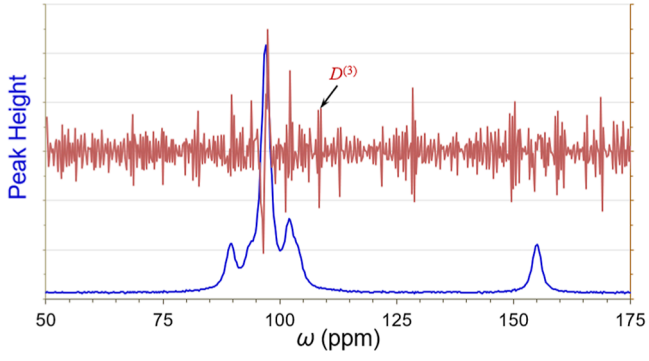

Figure 10. White Gaussian noise corrupted the $D^{(3)}$ derivative after it was mixed into the simulated overlapping band in Figure 2 at SNR = 20 (related to the smallest peak intensity = 0.500 and the sampling rate $4f_N$, equivalent to 512 data points).

https://doi.org/10.1021/acsomega.4c04536
ACS Omega 2024, 9, 36518−36530

the baseline noises in modern LC follow a normal distribution when the detection UV wavelength is fixed.[19] These denoising studies encouraged us to use the FT denoising technologies[3] to the simulated FT spectrum in Figure 10.

The simulated spectrum in Figure 10 (at SNR = 20 and sampling rate $4f_N$) was converted to the FID time signal by inverse FT and shown in Figure 11, where the FID was first

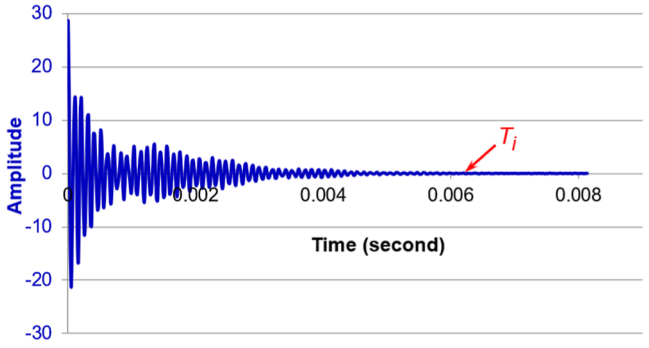

Figure 11. FID time signal was converted from the synthetic spectrum at sampling rate $4f_N$ and SNR = 20 in Figure 9 by inverse FT. Smoothing point of the boxcar function truncated at T_i = 0.00625 s.[3]

smoothed by a boxcar function truncated at T_i = 0.00625 s (the data points were set all to zero after T_i in Figure 11).[3] The smoothed FID was then decoded by FT with a band-pass filtering window (from 50 to 178 ppm) for denoising. After raising SNR = 40, we implemented the same procedures to smooth and denoise this FT spectrum at higher SNR. Similarly, a white Gaussian noise was generated in 2048 points and added into the same overlapping band simulated in a higher sampling rate $16f_N$ at SNR = 20 and SNR = 40, respectively. The same procedures were used to smooth and denoise the overlapping FT band simulated by the higher sampling rate $16f_N$. Figure 12

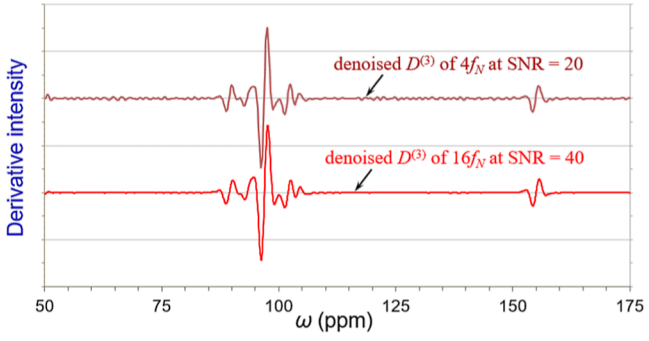

Figure 12. Denoised and smoothed spectrum of $D^{(3)}$ derivative spectra. Brown $D^{(3)}$ was obtained from the FID signal in Figure 11 at a sampling rate of $4f_N$ with SNR = 20. Red $D^{(3)}$ from sampling rate $16f_N$ with a SNR = 40. Their deconvolution results are shown in Table 9.

displays $D^{(3)}$ derivative spectra after smoothing and denoising of the simulated ^{13}C NMR overlapping bands in sampling rate $4f_N$ at SNR = 20 and in $16f_N$ at SNR = 40. It is gratifying to see that the noise was significantly reduced. The deconvolution results using $D^{(3)}$ are summarized in Table 9 for both sampling rates $4f_N$ and $16f_N$ at SNR = 20 and 40. Most of the denoised results are good for the additive white Gaussian noises. Comparing the deconvolution qualities in Table 9 to those simulated with no noise in Table 2, the higher sampling rate helps to reduce the deconvolution deviations. The noise residues strongly affected the deconvolutions of peak ω_5 because this peak is small (real intensity = 0.550) and closely overlapped (γ = 1.5 with ω_4). The absolute deviations of its deconvolutions were all over 26% (Table 9). Since the other peaks, ω_1 to ω_4, in the overlapping band had been deconvoluted well, we can easily isolate ω_5 with the reference peak ω_6 by removing the four deconvoluted peaks according to their found intensities A_j. Then the deconvolution accuracy of ω_5 was greatly boosted as isolated intensity A_5 is shown in Table 9.

It was notable that the SNR of NMR spectroscopy has been instantly enhanced by doubled and redoubled high magnetic fields.[20] However, the escalating magnetic fields of ^{13}C NMR spectroscopy do not resolve the overlapped bands well in biomolecular researches.[21] The deconvolution algorithms should play important roles in overlapping problems. If the noises are colored and contain low-frequency distortions, they should be treated with more effective and specific denoising technologies.[22]

5. COMPARISONS TO DECONVOLUTION SHARPENING ALGORITHMS

The derivatives perform the deconvolution point by point to FT spectral profiles, which is similar to curve fitting. Alternatively, the deconvolution of an overlapped band can be solved by deconvolution sharpening methods such as Fourier self-deconvolution (FSD), digital filters, and other algorithms.[13] There are numerous digital signal processing algorithms, linear or nonlinear.[23] These algorithms are very complicated and not discussed in this article because they usually require hundreds, even thousands, of iterative operations until a routine convergence can be obtained, for example, in Jasson's constrained iterative deconvolution.[23] A simple sharpening procedure was proposed in 1974 by den Harden and de Galan using the derivative FT principle to correct broadening effects and recover nondistorted peak heights.[24] They studied four broadening functions (triangle, Gaussian, Lorentzian, and exponential peak shapes). Since the deconvolution required the broadening width ≤ peak width of nondistorted bands, the overlapping bands could yield poor recovered peak heights.[24] Wahab et al. later refined den Harden and de Galan algorithm to deconvolute overlapping bands and to alter various peak tailings in HPLC. They obtained consistent area ratios for the benzene isotope triplet.[18,25] If FT peak shapes are asymmetric, then an extended FSD: Fourier complex self-deconvolution can also make them symmetric to sharpen the peaks.[3] Alternatively, our odd-order derivative method works differently in seeking independent intensities of the overlapped peaks before their overlap, which is similar to the curve fitting strategy in compliance with data integrity.

FSD is an effective algorithm used in FT spectroscopy to reduce peak width caused by instrumental broadening.[3] It is interesting to compare this conventional sharpening method with our new approach using odd-order derivatives. The same simulation data of ^{13}C NMR in previous section was used to implement the FSD algorithm for the classical apodization window of Bessel:[3] sampling rates $4f_N$ and $16f_N$ at SNR = 20 and 40, respectively. The same band-pass filtering and boxcar smoothing technologies were employed in the FSD study. We found that FSD provided very sharp peak shapes with good resolution. The FSD deconvolution results are specified in Table 10. Most of the peaks in the spectrum were recovered very well against the normalized reference peak ω_6 in Table 10. However, the recovered intensities of the small peaks ω_1 and ω_2 deviated

https://doi.org/10.1021/acsomega.4c04536
ACS Omega 2024, 9, 36518−36530

Table 9. Deconvolution Results by $D^{(3)}$ Derivative for the Simulated FT Spectrum with Additive White Gaussian Noises

peak ω_j (j = 1, 2, ..., 6)			ω_1	ω_2	ω_3	ω_4	ω_5	ω_6
overlapping degree γ			3.3	2.8	4.1	1.5	41.6	——
real intensity A_j			0.880	0.500	5.000	1.150	0.550	1.000
$4f_N$	SNR = 20	found A_j	0.905	0.557	5.145	1.170	0.389	1[a]
		% deviation	+2.8%	+11.4%	+2.9%	+1.3%	−29.3%	
		isolated A_5					0.579	1[a]
		% deviation					+5.3%	
	SNR = 40	found A_j	0.870	0.528	5.075	1.142	0.394	1[a]
		% deviation	−1.1%	+5.6%	+1.5%	−0.7%	−28.4%	
		isolated A_5					0.592	1[a]
		% deviation					+7.6%	
$16f_N$	SNR = 20	found A_j	0.891	0.507	5.064	1.134	0.404	1[a]
		% deviation	+1.3%	+1.4%	+1.3%	−1.4%	−26.5%	
		isolated A_5					0.540	1[a]
		% deviation					−1.8%	
	SNR = 40	found A_j	0.909	0.513	5.055	1.125	0.405	1[a]
		% deviation	+3.3%	+2.6%	+1.1%	−2.2%	−26.4%	
		isolated A_5					0.543	1[a]
		% deviation					−1.3%	

[a]Peak ω_6 is normalized to one in the intensity evaluation.

Table 10. Results of FSD for the Simulated FT Spectrum with Additive White Gaussian Noises

peak ω_j (j = 1, 2, ..., 6)			ω_1	ω_2	ω_3	ω_4	ω_5	ω_6
overlapping degree γ			3.3	2.8	4.1	1.5	41.6	–
real intensity A_j			0.880	0.500	5.000	1.150	0.550	1.000
$4f_N$	SNR = 20	found A_j	0.893	0.542	4.849	1.120	0.520	1[a]
		% deviation	+1.5%	+8.4%	−3.0%	−2.6%	−5.5%	
	SNR = 40	found A_j	0.925	0.565	5.131	1.184	0.562	1[a]
		% deviation	+5.1%	+13.0%	+2.6%	+3.0%	+2.2%	
$16f_N$	SNR = 20	found A_j	0.811	0.503	4.902	1.113	0.525	1[a]
		% deviation	−7.8%	+0.6%	−2.0%	−3.2%	−4.5%	
	SNR = 40	found A_j	0.817	0.512	4.915	1.111	0.527	1[a]
		% deviation	−7.2%	+2.4%	−1.7%	−3.4%	−4.2%	

[a]Peak ω_6 is normalized to one in the intensity evaluation.

from 7.2 to 13%, depending on where the noise-residue remains. The recovered ω_5 intensity is superior to that evaluated by the $D^{(3)}$ derivative approach because the peak widths of the overlapping band have been narrowed by a factor from the FSD (see a typical FSD spectrum shown in Section S5 of the Supporting Information). Nevertheless, some of them are not as close to their real values than the $D^{(3)}$ derivative approach (such as ω_3 and ω_4) because the dynamic range of FSD for different peak intensities is not as wide as the derivative algorithms. The major issue arises from the apodization, not the FSD method. Even for a group of pure sinusoid signals with well separations, their peak ratios would have obvious deviations by the apodization, either with Bessel, Gaussian, exponential, or 3-term Blackman-Harris or other commonly used windows. The derivatives can provide wider dynamic ranges (intensity ratios up to 10:1) for the regular exponential decay signals in FT spectroscopy (referring to Section S7 of Supporting Information for a representative FSD spectrum from the simulated overlapping band in Table 9).

Because NMR experiments employed many different pulse programs to yield nuclei relaxation processes, the FSD algorithm was generally used in infrared spectroscopy and Raman spectroscopy more than in NMR spectroscopy.[3] Wahab and O'Haver developed a modified FSD method to effectively suppress high-frequency noises by adding a small constant distribution or other symmetric distribution to the broadening related response during inverse FT.[26] They provided a more precise strategy to trace the appearance of the noises and suppress them. Kauppinen's derivative FSD can further narrow the peak width.[3] Shan et al. furthermore implemented iterative operations to enhance the performance of Kauppinen's derivative FSD, and applied them to near-infrared and middle-infrared spectroscopy for quantitative analysis of the Albiflorin dataset and γ-Polyglutamic acid fermentation dataset.[27] After the above comparisons, we need to emphasize that our goal is to find independent peak intensities of overlapping FT bands quantitatively using the odd-order derivatives.

6. RESULTS AND DISCUSSION

FT spectrum profiles demonstrate typical bell shapes, narrow tops, and broad bottoms. We naturally assumed that the intensity dilations of the overlapping peaks should be relatively larger than shifting their peak centers. An odd-order derivative normally exhibits four obvious characteristics: two primary maximums, an interval between the two maximums, and a zero-crossing point. The responses of the PMRs are more susceptible to variations of the overlapping degrees compared with the interval ratios and area ratios of the primary derivative peaks. Implementation of the stepwise superimposition offers a differential approach on a FT spectrum to refine its resolution.[1,2]

https://doi.org/10.1021/acsomega.4c04536
ACS Omega 2024, 9, 36518−36530

This approach contributes three benefits to FT spectroscopy: (1) sharp resolution, (2) peak shapes unimportant, and (3) the superimposed intensity coincident with amplitude of its sinusoidal time signal. In this work, we used odd-order derivatives to evaluate the independent heights of the overlapping spectrum peaks toward quantitative analysis of FT spectroscopy. This simple procedure improves spectral resolutions and analytical precisions when facing the performance ceilings of any FT spectrometer on hand. The PM gaps of odd-order derivatives should be "convergent", gradually decreasing with growing derivative orders. Third- and fifth-order derivatives are most suitable to the deconvolution. Higher (>5th) odd-order derivatives of the overlapping peaks often reverted to "divergent" in our simulation studies as their PM gaps became wider than expected.

Derivative spectra are excellent remedial measurements of conventional spectroscopy and spectrometry, raising analytical performance without substantially upgrading instrumental hardware. There have been few monographs devoted to derivative spectroscopy up until now.[4,28−31] Rojas, Ojeda, and Karpińska et al. had written a series of reviews about derivative spectrophotometry, covering the developments and applications in six decades, including odd-order derivatives.[32−49] Karpińska deems odd-order derivatives as optimal in the application of the Savitzky−Golay algorithm for the generation of derivative spectra.[47] Dehnavi et al. compared derivative methods used in hyperspectral analysis of two mineral groups totaling 28 targets and odd-order derivatives were overwhelmingly preferred (odd/even = 13/7) in remote sensing studies after excluding 8 zero-orders as a nonderivative approach.[50] Cameron and Moffatt perceived as early as 1986: "the experimental SNR is such that the optimum result is intermediate between the 2nd and 4th", despite their endeavors to truncate smoothly even-order derivative FT spectra in terms of the weighting functions.[51]

Higher odd-order derivatives nowadays are constantly employed in FT spectroscopy.[52−71] Most applications of derivative spectroscopy are utilized for complex chemical mixtures because of their analytical specificity and selectivity. In this work, we made use of odd-order derivatives to evaluate the independent intensities of overlaying FT bands for various peak profiles, including magnitude-mode. Even-order derivatives may not be adequate for evaluating the overlapped magnitude peaks because of their nonadditive nature.[14] Since signal generations of conventional FT spectroscopy/spectrometry involve retardation of optical interferometers or radio-frequency pulses, their reproducibility cannot be as good as steady optical or charge detections. Thus, the deconvolution of overlapping FT bands with a reference peak (either by choosing an independent peak or spiking with an internal standard) can offset the detection bias and benefit evaluation accuracy and precision when using odd-order derivatives. It is well-known that the internal standard strategy has been used in the reference deconvolution of FT-NMR spectroscopy to calibrate the peak profile via time-frequency transformation.[72] If a FT spectrum is used instead of taking the derivative(s) first and then obtaining its magnitude spectrum, such a procedure does not distinguish between odd- and even-order derivatives[7−9] and is beyond our discussion scope.

The wavelet transform is closely related to FT and is good at threshold denoising by localization.[73] In a recent comparative study with normalization, standard normal variate, Savitzky−Golay filter, first-order and second-order derivatives, and wavelet transform manifested the optimal deconvolution resulted in removing noises for both FT infrared spectroscopy and Raman spectroscopy.[74] The other denoising techniques are also available to spectroscopies.[22,75,76] Magnification of spectral noises by the higher-order derivatives consequently is not important with respect to issues in pace with state-of-the-art technologies. Intrinsic disturbances such as phase shifting, Gibbs effect, and derivative satellites are crucial to derivative spectroscopy.[4]

Fractional-order derivatives had been used to evaluate overlapping spectrum peaks.[4] Since the primary maximums of the fractional-order derivatives are not linear functions of FWHM2σ,[77,78] they consume more calculation times in the deconvolution of the overlapping peaks. The overlapping spectra are enriched from the overlapping degrees, peak intensities, and peak populations together, which belong to fraction-order systems. Fractional-order derivatives are suitable for specified and plain targets. Thus, they are widely used for hyperspectral remote sensing.[79] Alternatively, a change of sampling rates or averaging the results of the convergent odd-order derivatives would be easier to manipulate.

Functionally enhanced derivative spectroscopy is a spectacular invention that can greatly reduce FWHM of the spectrum peaks.[49] This new tool normalizes individual overlapping peaks against the maximum apparent peak intensity in a spectrum. It strongly relies on specified spectra with prior knowledge about peak identities. Because the effects of the overlapping degrees and derivative satellites have not been studied methodically, it had to artificially add a scale factor to adjust the deconvoluting intensities.[80]

Curve fitting algorithms are the most classical deconvolution methods of FT spectroscopy.[81] They are widely used in various spectroscopies.[13] Almost all acquired data in a spectrum is joined together in curve fitting evaluations. Many advanced curve fitting procedures for spectroscopic deconvolution have been developed very recently with prevalent computer programs like Python,[68] R-language,[82] Matlab,[83] and deep learning approach.[84] A major problem of the curve fitting is the difficulty in locating deviations of physical processes in peak intensity measurements.[85] The PMRs of odd-order derivatives are useful in calculating initial peak intensities, which can help greatly in improving the accuracy of the curve fitting procedures.

Sometimes broad peaks may appear by FT spectroscopy. Poor shimming, nonhomogeneous sampling, nonfirst-order coupling, and dynamic influence would cause broadening effects in NMR spectroscopy.[86] These sophisticated phenomena involve optimization in NMR measurements and instrumentation. In the presence of intermolecular hydrogen bonding, broad peaks will appear in FT infrared spectroscopy, such as hydroxyl, amine, amide functional groups, and polymers correlated highly with vibration modes and chemical environments.[87] Comparatively, spectrum peak distortion in FT mass spectrometry can be minimized by appropriate experimental design and calibration procedures for ion detection under high vacuum conditions.[88] Major broadening peaks of FT mass spectrometry originate from space charge interaction and ion-neutral collision.[89,90] We recommend deconvoluting the broad peaks whenever they are distinguishable by derivatives in steady state situations. If not distinguishable derivatively, the peaks can be manifested with their differential baselines by the differentially superimposed FT approach.[1,2] When signal intensities are weak relative to noise levels and instrumental distortions, often in FT-Raman spectroscopy, we should lower our expectations in a quantitative deconvolution as the general guides.[17]

https://doi.org/10.1021/acsomega.4c04536
ACS Omega 2024, 9, 36518−36530

7. CONCLUSIONS

We exploited new procedures to deconvolute overlapping peaks using odd-order derivatives toward quantitative evaluation of their independent (real) intensities according to the characteristics of FT spectroscopy. Odd-order derivatives of Lorentzian-type profiles have dispersive maxima and smaller derivative satellites. Their dispersive maxima can respond to different overlapping influences. It is applicable to cast off the overlapping effect for the most common Lorentzian peaks of FT spectroscopy. The PMRs of the odd-order derivatives are desirable in deconvoluting the overlapping magnitude peaks. With the aid of a well separated peak as a crux, independent intensities of the overlapping peak in the same spectrum can be estimated. Our approaches are simple and robust. Their evaluation results are good in simulation studies and could provide more accurate and precise deconvolutions when comparing them to even-order derivatives. Deconvolutions to Gaussian, Voigt, and Tsallis peak shapes with odd-order derivatives have slightly more deviations than Lorentzian and magnitude profiles. Nevertheless, our new approach should be improved to cover more complicated overlapping scenarios such as different peak widths, determinations involving peak areas, and asymmetric peak shapes.

Although derivative approaches play an important role in complicated measurements, researches, and discoveries, according to our best knowledge regarding pharmaceutical analysis, they were rarely approved as official compendial methods.[91] Spectral analysis always attempts success in distinguishable determination physically and/or chemically. The new derivative approaches of FT spectroscopy should further reduce routine residue evaluation errors. Our study provides substantial support for the odd-order derivative analysis and an explanation for why there have been numerous applications over the last several years.[52−71] We believe that derivative spectroscopy can be reliably used to analyze specific targets with compliant validation.

■ ASSOCIATED CONTENT

Supporting Information

The Supporting Information is available free of charge at https://pubs.acs.org/doi/10.1021/acsomega.4c04536.

Intensity-corrected superimposed FT NMR spectrum (XLSX)

Superimposing peak; stepwise superimpose principle; formulas of high-order derivatives; simulation of ^{13}C NMR signal; Excel calculations of the deconvolutions for the simulation and real NMR spectrum of ethylbenzene; Python codes of white Gaussian noises; and sharpening by FSD (PDF)

■ AUTHOR INFORMATION

Corresponding Author

Shu-Ping Chen − *Nexus Scitech Centre of Canada, Richmond Hill, Ontario L4B 3R7, Canada; Fujian Superimposegraph Co., Ltd, Fuzhou, Fujian 350013, China;* orcid.org/0009-0008-4460-9404; Email: shuping.chen@fjsuperimpose.com

Authors

Sandra M. Taylor − *Department of Civil Engineering, Camosun College (Interurban Campus), Victoria, British Columbia V9E 2C1, Canada*

Sai Huang − *Fujian Superimposegraph Co., Ltd, Fuzhou, Fujian 350013, China*

Baoling Zheng − *Fujian Superimposegraph Co., Ltd, Fuzhou, Fujian 350013, China*

Complete contact information is available at: https://pubs.acs.org/10.1021/acsomega.4c04536

Author Contributions

‖S.-P.C. and S.M.T. contributed equally. S.H. and B.Z. worked on the related software and have given their approval to the final version of the manuscript.

Funding

This work received no specific grant from any funding agency in the public, commercial, or not-for-profit sectors.

Notes

The authors declare no competing financial interest.

■ ACKNOWLEDGMENTS

We appreciate our families' supporting this work during the COVID pandemic.

■ REFERENCES

(1) Chen, S.; Huang, S.; Zheng, B.; Comisarow, M. B. Superimpose Fourier Transform and Applications in Spectroscopy and Imaging. In *Imaging and Applied Optics Congress*; OSA Technical Digest, 2020; p ITu4G.7..

(2) Chen, S.; Huang, S.; Zheng, B. Derivative Fourier transform spectroscopy and imaging using stepwise superimpose strategy. *International Conference on Optoelectronic Information and Computer Engineering (OICE)*; Proceedings of the SPIE, 2022; p 1230805.

(3) Kauppinen, J.; Partanen, J. *Fourier Transforms in Spectroscopy*; Wiley VCH: Berlin, 2001; Chapters 1, 11 and 12.

(4) Dubrovkin, J. *Derivative Spectroscopy*; Cambridge Scholars: Newcastle upon Tyne, 2021.

(5) Anderssen, R. S.; Hegland, M. Derivative spectroscopy − An enhanced role for numerical differentiation. *J. Integral Equ. Appl.* **2010**, *22* (3), 355−367.

(6) Owen, A. J. *Uses of Derivative Spectroscopy: Application Note*; Agilent Technologies, Publication Number 5963−3940E, 1995. CorpusID: 5935801.

(7) Belkić, D.; Belkić, K. Review of recent applications of the conventional and derivative fast Padé transform for magnetic resonance spectroscopy. *J. Math. Chem.* **2019**, *57*, 385−464.

(8) Belkić, D.; Belkić, K. Exact quantification by the nonparametric fast Padé transform using only shape estimation of high-order derivatives of envelopes. *J. Math. Chem.* **2018**, *56*, 268−314.

(9) Belkić, D.; Belkić, K. Explicit extraction of absorption peak positions, widths and heights using higher order derivatives of total shape spectra by nonparametric processing of time signals as complex damped multi-exponentials. *J. Math. Chem.* **2018**, *56*, 932−977.

(10) Marshall, A. G.; Verdun, F. R. *Fourier Transforms in NMR, Optical and Mass Spectrometry: A User's Handbook*; Elsevier: Amsterdam, 1990.

(11) Vandeginste, B. G. M.; De Galan, L. Critical evaluation of curve fitting in infrared spectrometry. *Anal. Chem.* **1975**, *47* (13), 2124−2132.

(12) Gorkovskiy, A.; Thurber, K. R.; Tycko, R.; Wickner, R. B. Locating folds of the in-register parallel β-sheet of the Sup35p prion domain infectious amyloid. *Proc. Natl. Acad. Sci. U.S.A.* **2014**, *111* (43), E4615−E4622.

(13) Dubrovkin, J. *Mathematical Processing of Spectral Data in Analytical Chemistry: a Guide to Error Analysis*; Cambridge Scholars, Newcastle upon Tyne, 2018; Part IV Chapter 1 and Chapter 2.

(14) Lee, J. P.; Comisarow, M. B. The phase dependence of magnitude spectra. *J. Magn. Reson.* **1987**, *72* (1), 139−142.

(15) Bruker BioSpin END. *AVANCE Beginners Guide*, version 7; Bruker, 2018; pp 18−20.

(16) Shimizu, T.; Hashi, K.; Goto, A.; Tansyo, M.; Kiyoshi, T.; Matsumoto, S.; Wada, H.; Fujito, T.; Hasegawa, K.-i.; Kirihara, N.; Suematsu, H.; Kida, Y.; Yoshikawa, M.; Miki, T.; Ito, S.; Hamada, M.; Hayashi, S. Overview of the development of high-resolution 920 MHz NMR in NIMS. *Phys. B* **2004**, *346/347*, 528−530.
(17) Meyer, C.; Seiler, P.; Bies, C.; Cianciulli, C.; Wätzig, H.; Meyer, V. R. Minimum required signal-to-noise ratio for optimal precision in HPLC and CE. *Electrophoresis* **2012**, *33* (11), 1509−1516.
(18) Wahab, M. F.; Gritti, F.; O'Haver, T. C. Discrete Fourier transform techniques for noise reduction and digital enhancement of analytical signals. *TrAC, Trends Anal. Chem.* **2021**, *143*, 116354.
(19) Kotani, A.; Watanabe, R.; Hayashi, Y.; Machida, K.; Hakamata, H. Statistical reliability of a relative standard deviation of chromatographic peak area estimated by a chemometric tool based on the FUMI theory. *J. Pharm. Biomed. Anal.* **2024**, *237*, 115777.
(20) Felli, I. C.; Pierattelli, R. 13C Direct detected NMR for challenging systems. *Chem. Rev.* **2022**, *122*, 9468−9496.
(21) Callon, M.; Malär, A. A.; Pfister, S.; Římal, V.; Weber, M. E.; Wiegand, T.; Zehnder, J.; Chávez, M.; Cadalbert, R.; Deb, R.; Däpp, A.; Fogeron, M.-L.; Hunkeler, A.; Lecoq, L.; Torosyan, A.; Zyla, D.; Glockshuber, R.; Jonas, S.; Nassal, M.; Ernst, M.; Böckmann, A.; Meier, B. H. Biomolecular solid state NMR spectroscopy at 1200 MHz: the gain in resolution. *J. Biomol. NMR* **2021**, *75*, 255−272.
(22) Koziol, P.; Raczkowska, M. K.; Skibinska, J.; Urbaniak-Wasik, S.; Paluszkiewicz, C.; Kwiatek, W.; Wrobel, T. P. Comparison of spectral and spatial denoising techniques in the context of high definition FT-IR imaging hyperspectral data. *Sci. Rep.* **2018**, *8* (1), 14351. *Sci. Rep.* **2020**, *10*(1), 5699..
(23) *Deconvolution of Images and Spectra*, 2ed.; Jansson, P. A., Ed.; Academic PressSan Diego, 1997.
(24) Den Harder, A.; de Galan, L. Evaluation of a method for real-time deconvolution. *Anal. Chem.* **1974**, *46* (11), 1464−1470.
(25) Wahab, M. F.; O'Haver, T. C.; Gritti, F.; Hellinghausen, G.; Armstrong, D. W. Increasing chromatographic resolution of analytical signals using derivative enhancement approach. *Talanta* **2019**, *192*, 492−499.
(26) Wahab, M. F.; O'Haver, T. C. Peak deconvolution with significant noise suppression and stability using a facile numerical approach in Fourier space. *Chemom. Intell. Lab. Syst.* **2023**, *235*, 104759.
(27) Shan, P.; Liu, J.; He, Z.; Peng, S.; Wang, F.; Liu, C.; Zhou, Z. A novel infrared spectral preprocessing method based on self-deconvolution and differentiation in the frequency domain. *Vib. Spectrosc.* **2023**, *127*, 103562.
(28) Allesia, M.; Gillespie, Jr. *Manual of Spectrofluorometric and Spectrophotometric Derivative Experiments*; CRC: Boca Raton, 1994.
(29) Talsky, G. *Derivative Spectrophotometry: Low and Higher Order*; VCH: New York, 1994.
(30) Saakov, V. S.; Drapkin, V. Z.; Krivchenko, A. I.; Rozengart, E. V.; Bogachev, Y. V.; Knyzev, M. N. *Derivative Spectrophotometry and electron Spin Resonance (ESR) Spectroscopy for Ecological and Biological Questions*; Springer-Verlag: Wien, 2013.
(31) Saakov, V. S.; Krivchenko, A. I.; Rozengart, E. V.; Danilova, I. G. *Derivative Spectrophotometry and PAM-Fluorescence in Comparative Biochemistry*; Springer: Switzerland, 2015.
(32) Talsky, G.; Mayring, L.; Kreuzer, H. High-resolution, higher-order UV/VIS derivative spectrophotometry. *Angew. Chem., Int. Ed. Engl.* **1978**, *17* (11), 785−799.
(33) Dixit, L.; Ram, S. Quantitative Analysis by Derivative Electronic Spectroscopy. *Appl. Spectrosc. Rev.* **1985**, *21* (4), 311−418.
(34) Rojas, F. S.; Ojeda, C. B.; Pavon, J. M. C. Derivative ultraviolet-visible region absorption spectrophotometry and its analytical applications. *Talanta* **1988**, *35* (10), 753−761.
(35) Demetriades-Shah, T. H.; Steven, M. D.; Clark, J. A. High resolution derivative spectra in remote sensing. *Remote Sens. Environ.* **1990**, *33* (1), 55−64.
(36) Ojeda, C. B.; Rojas, F. S.; Pavon, J. M. C. Recent developments in derivative ultraviolet/visible absorption spectrophotometery. *Talanta* **1995**, *42* (9), 1195−1214.
(37) Kuś, S.; Marczenko, Z.; Obarski, N. Derivative UV-VIS spectrophotometry in analytical chemistry. *Chem. Anal.* **1996**, *41*, 899−929.
(38) Popovic, G. V.; Pfendt, L. B.; Stefanovic, V. M. Analytical application of derivative spectrophotometry. *J. Serb. Chem. Soc.* **2000**, *65* (7), 457−472.
(39) Bosch Ojeda, C.; Sanchez Rojas, F. Recent developments in derivative ultraviolet/visible absorption spectrophotometry. *Anal. Chim. Acta* **2004**, *518* (1−2), 1−24.
(40) Karpiska, J. Derivative spectrophotometry recent applications and directions of developments. *Talanta* **2004**, *64* (4), 801−822.
(41) El-Sayed, A.-A. Y.; El-Salem, N. A. Recent developments of derivative spectrophotometry and their analytical applications. *Anal. Sci.* **2005**, *21* (6), 595−614.
(42) Rojas, F. S.; Ojeda, C. B. Recent development in derivative ultraviolet/visible absorption spectrophotometry: 2004−2008, A review. *Anal. Chim. Acta* **2009**, *635* (1), 22−44.
(43) Ortiz, J. D. Application of Visible/near Infrared derivative spectroscopy to Arctic paleoceanography. *IOP Conf. Ser. Earth Environ. Sci.* **2011**, *14*, 012011.
(44) Karpińska, J. Basic Principles and analytical application of derivative spectrophotometry. In *Macro to Nano Spectroscopy*; Uddin, J., Ed.; InTech: Croatia, 2012; pp 253−268.
(45) Bosch Ojeda, C.; Sanchez Rojas, F. Recent applications in derivative ultraviolet/visible absorption spectrophotometry: 2009−2011. *Microchem. J.* **2013**, *106*, 1−16.
(46) Parmar, A.; Sharma, S. Derivative UV-Vis absorption spectra as an invigorated spectrophotometric method for spectral resolution and quantitative analysis: Theoretical aspects and analytical applications: A review. *TrAC, Trends Anal. Chem.* **2016**, *77*, 44−53.
(47) Redasani, V. K.; Patel, P. R.; Marathe, D. Y.; Chaudhari, S. R.; Shirkhedkar, A. A.; Surana, S. J. A review on derivative uv-spectrophotometry analysis of drugs in pharmaceutical formulations and biological samples review. *J. Chil. Chem. Soc.* **2018**, *63* (3), 4126−4134.
(48) Karpińska, J. Spectrophotometry—Derivative Spectroscopy; In *Encyclopedia of Analytical Science*, 3ed, Vol. *9*; Worsfold, P., Townshend, A., Poole, C., Miró, M., Eds.; Elsevier: Amsterdam, 2019; pp 214−220.
(49) Palencia, M.; Garcés-Villegas, V.; Restrepo, D. F.; Martínez, J. M.; Anaya-Tatis, L. R.; Combatt, E. M. Functionally-enhanced derivative spectroscopy (FEDS): a powerful tool to increase of spectral resolution in the mid-infrared advanced analysis of complex samples−a mini review. *J. Appl. Biotechnol. Bioeng.* **2020**, *7* (1), 43−46.
(50) Dehnavi, S.; Maghsoudi, Y.; Zoej, M. J. V.; Baniadam, F. High-order derivative spectrum in hydrothermally altered minerals discrimination. *J. Appl. Biotechnol. Bioeng.* **2015**, *9*, 096086.
(51) Cameron, D. G.; Moffatt, D. J. A generalized approach to derivative spectroscopy. *Appl. Spectrosc.* **1987**, *41* (4), 539−544.
(52) Rele, R. V. Derivative spectrophotometric estimation of amoxicillin trihydrate and carbocisteine by third order derivative spectroscopy method in combined dosage form. *Res. J. Pharm. Technol.* **2017**, *10* (6), 1758−1761.
(53) Dehnavi, S.; Maghsoudi, Y.; Valadanzoej, M. Using spectrum differentiation and combination for target detection of minerals. *Int. J. Appl. Earth Obs. Geoinf.* **2017**, *55*, 9−20.
(54) Usharani, N.; Divya, K.; Vvs, A. Development and validation of UV-derivative spectroscopic and RP-HPLC methods for the determination of amlodipine besylate and valsartan in tablet dosage form and comparison of the developed methods by student's t-test. *Indian J. Pharm. Educ. Res.* **2017**, *51* (4S), S776−S782.
(55) Müllerová, J.; Šutta, P.; Prušáková, L. Derivative optical spectroscopy of thin films of alkaline-earth titanates: Critical points. *AIP Conf. Proc.* **2018**, *1996*, 020030.
(56) Kovalenko, A. V.; Plakhtiy, E. G.; Vovk, S. M. Application of derivative spectroscopy method to photoluminescence in ZnS:Mn nanocrystals. *Ukr. J. Phys. Opt.* **2018**, *19* (3), 133−140.
(57) Wang, Q.; Jin, J.; Sonobe, R.; Chen, J. M. Derivative Hyperspectral Vegetation Indices in Characterizing Forest Biophysical and Biochemical Quantities. In *Hyperspectral Indices and Image*

https://doi.org/10.1021/acsomega.4c04536
ACS Omega 2024, 9, 36518−36530

Classifications for Agriculture and Vegetation. Thenkabail, P. S., Lyon, J. A., Huete, A., Eds.; CRC Press: Roca Raton, 2018; Vol. 2; pp 27−63, Chapter 2.
(58) Halboos, M. H.; Ammar Sayhood, A.; Ala'a Hussein, T. Determination celiprolol hydrochloride drug by used zero, first, second and third order derivative and peak area spectrophotometry method in its pure form and in pharmaceutical tablets. *J. Phys.: Conf. Ser.* **2019**, *1294*, 052035.
(59) Simion, I. M.; Sârbu, C. The impact of the order of derivative spectra on the performance of pattern recognition methods. Classification of medicinal plants according to the phylum. *Spectrochim. Acta, Part A* **2019**, *219*, 91−95.
(60) Kovalenko, O. V.; Plakhtii, Ye. G.; Khmelenko, O. V.; Vorovsky, V. Yu. The analysis of the EPR spectra in ZnO: Mn nanocrystals using the derivative spectroscopy method. *J. Phys. Electron.* **2019**, *27* (2), 89−92.
(61) Alekhya, B.; Sindhusha, M.; Raul, S. K.; Padhy, G. K. A new validated third order derivative spectroscopic method for simultaneous estimation of metoprolol succinate and ramipril in tablet dosage form. *Int. J. Pharm. Pharm. Sci.* **2020**, *12* (5), 54−59.
(62) Hu, Y.; Zhao, D.; Qin, Y.; Wang, X. An order determination method in direct derivative absorption spectroscopy for correction of turbidity effects on COD measurements without baseline required. *Spectrochim. Acta, Part A* **2020**, *226*, 117646.
(63) Liu, S.; Zheng, J.; Fang, Y. Obrechkoff two-step method fitted with Fourier spectrum for undamped Duffing equation. *J. Math. Chem.* **2020**, *58* (3), 717−734.
(64) Elsonbaty, A.; Hasan, M. A.; Eissa, M. S.; Hassan, W. S.; Abdulwahab, S. Synchronous spectrofluorimetry coupled with third-order derivative signal processing for the simultaneous quantitation of telmisartan and chlorthalidone drug combination in human plasma. *J. Fluoresc.* **2021**, *31* (1), 97−106.
(65) Amirkhan, F.; Gratuze, M.; Ropagnol, X.; Ozaki, T.; Nabki, F.; Blanchard, F. Terahertz time-domain derivative spectrometer using a large-aperture piezoelectric micromachined device. *Opt. Express* **2021**, *29* (14), 22096−22107.
(66) Wang, C.; Yi, X.; Kim, M.; Yang, Q. B.; Han, R. A terahertz molecular clock on CMOS using high-harmonic-order interrogation of rotational transition for medium-/long-term stability enhancement. *IEEE J. Solid-State Circuits* **2021**, *56* (2), 566−580.
(67) Pineau, M.; Mathian, M.; Baron, F.; Rondeau, B.; Le Deit, L.; Allard, T.; Mangold, N. Estimating kaolinite crystallinity using near-infrared spectroscopy: implications for its geology on Earth and Mars. *Am. Mineral.* **2022**, *107* (8), 1453−1469.
(68) Ginsburg, A.; Sokolov, V.; de Val-Borro, M.; Rosolowsky, E.; Pineda, J. E.; Sipőcz, B. M.; Henshaw, J. D.; Henshaw, J. D. Pyspeckit: A spectroscopic analysis and plotting package. *Astron. J.* **2022**, *163*, 291.
(69) Jin, J.; Huang, N.; Huang, Y.; Yan, Y.; Zhao, X.; Wu, M. Proximal remote sensing-based vegetation indices for monitoring mango tree stem sap flux density. *Remote Sens.* **2022**, *14*, 1483.
(70) Kim, M.; Wang, C.; Yi, L.; Lee, H.-S.; Han, R. A sub-THz CMOS molecular clock with 20 ppt stability at 10,000 s based on dual-loop spectroscopic detection and digital frequency error integration. RMo3A-1. In *2022 IEEE Radio Frequency Integrated Circuits Symposium (RFIC)*; IEEE, 2022; pp 115−118.
(71) Jin, J.; Wu, M.; Song, G.; Wang, Q. Genetic algorithm captured the informative bands for partial least squares regression better on retrieving leaf nitrogen from hyperspectral reflectance. *Remote Sens.* **2022**, *14*, 5204.
(72) Ebrahimi, P.; Viereck, N.; Bro, R.; Engelsen, S. B. Chemometric Analysis of NMR Spectra. In *Modern Magnetic Resonance*; Webb, G. A., Ed., 2ed.; Springer: Cham, 2018; pp 1654−1657.
(73) Thuillard, M. *Wavelets in Soft Computing*; 2ed.; World Scientific: Singapore, 2023.
(74) Yang, X.; Wu, Z.; Ou, Q.; Qian, K.; Jiang, L.; Yang, W.; Shi, Y.; Liu, G. Diagnosis of lung cancer by FTIR spectroscopy combined with Raman spectroscopy based on data fusion and Wavelet transform. *Front. Chem.* **2022**, *10*, 810837.
(75) Laurent, G.; Woelffel, W.; Barret-Vivin, V.; Gouillart, E.; Bonhomme, C.; Bonhomme, C. Denoising applied to spectroscopies-part I: concept and limits. *Appl. Spectrosc. Rev.* **2019**, *54* (7), 602−630.
(76) Laurent, G.; Gilles, P.-A.; Woelffel, W.; Barret-Vivin, V.; Gouillart, E.; Bonhomme, C. Denoising applied to spectroscopies − Part II: Decreasing computation time. *Appl. Spectrosc. Rev.* **2020**, *55* (3), 173−196.
(77) Kharintsev, S. S.; Salakhov, M. Kh. A simple method to extract spectral parameters using fractional derivative spectrometry. *Spectrochim. Acta, Part A* **2004**, *60* (8−9), 2125−2133.
(78) Li, Y.-l.; Tang, H.-q.; Chen, H.-x. Fractional-order derivative spectroscopy for resolving simulated overlapped Lorenztian peaks. *Chemom. Intell. Lab. Syst.* **2011**, *107* (1), 83−89.
(79) Li, C.; Xiao, Z.; Liu, Y.; Meng, X.; Li, X.; Wang, X.; Li, Y.; Zhao, C.; Ren, L.; Yang, C.; Jiao, Y. Hyperspectral estimation of winter wheat leaf water content based on fractional order differentiation and continuous wavelet transform. *Agronomy* **2022**, *13*, 56.
(80) Palencia, M. Functionally-enhanced derivative spectroscopy (FEDS): A methodological approach. *J. Sci. Technol. Appl.* **2020**, *9*, 29−34.
(81) Griffiths, P. R.; Pierce, J. A.; Hongjin, G. Curve Fitting and Fourier Self-Deconvolution for the Quantitative Representation of Complex Spectra. In *Computer-Enhance Analytical Spectroscopy*; Meuzelaar, H. L. C., Isenhour, T. L., Eds.; Plenum: New York, 1987; Vol. 2, pp 29−54.
(82) Häckl, M.; Tauber, P.; Schweda, F.; Zacharias, H. U.; Altenbuchinger, M.; Oefner, P. J.; Gronwald, W. An R-package for the deconvolution and integration of 1D NMR data: MetaboDecon1D. *Metabolites* **2021**, *11*, 452.
(83) Schulze, H. G.; Rangan, S.; Vardaki, M. Z.; Blades, M. W.; Turner, R. F. B.; Piret, J. M. Critical Evaluation of Spectral Resolution Enhancement Methods for Raman Hyperspectra. *Appl. Spectrosc.* **2022**, *76* (1), 61−80.
(84) Schmid, N.; Bruderer, S.; Paruzzo, F.; Fischetti, G.; Toscano, G.; Graf, D.; Fey, M.; Henrici, A.; Ziebart, V.; Heitmann, B.; Grabner, H.; Wegner, J. D.; Sigel, R. K. O.; Wilhelm, D. Deconvolution of 1D NMR spectra: A deep learning-based approach. *J. Magn. Reson.* **2023**, *347*, 107357.
(85) Matviychuk, Y.; Steimers, E.; von Harbou, E.; Holland, D. J. Improving the accuracy of model-based quantitative nuclear magnetic resonance. *Magn. Reson.* **2020**, *1* (2), 141−153.
(86) Richards, S. A.; Hollerton, J. C. *Essential Practical NMR for Organic Chemistry*, 2ed.; Wiley: Hoboken, 2023.
(87) Thompson, J. M. *Infrared Spectroscopy*; Pan Stanford: Singapore, 2018.
(88) Marshall, A. G.; Hendrickson, C. L. Fourier transform ion cyclotron resonance detection: Principles and experimental configurations. *Int. J. Mass Spectrom.* **2002**, *215* (1−3), 59−75.
(89) Chen, S.-P.; Comisarow, M. B. Modelling coulomb effects in Fourier-transform ion cyclotron resonance mass spectrometry by charged disks and charged cylinders. *Rapid Commun. Mass Spectrom.* **1992**, *6* (1), 1−3.
(90) James, V. K.; Sanders, J. D.; Aizikov, K.; Fort, K. L.; Grinfeld, D.; Makarov, A.; Brodbelt, J. S. Advancing Orbitrap measurements of collision cross sections to multiple species for broad applications. *Anal. Chem.* **2022**, *94* (45), 15613−15620.
(91) Commentary USP−NF 2022 Issue 3, June 1, 2022.

https://doi.org/10.1021/acsomega.4c04536
ACS Omega 2024, 9, 36518−36530